Chapter 5

Photoinduced Coherent Charge Transfer

5.0.1 ABSTRACT

Theoretical and spectroscopic evidence of coherent oscillatory behaviour associated to photoinduced charge transfer has been reported both in complex biological environments as well as in biomimetic models for artificial photosynthesis. Here we consider a biomimetic model to investigate this process in real-time simulations based on Ehrenfest dynamics. The Ehrenfest formalism allows for a detailed analysis of how photon-to-charge conversion is promoted by a coupling of the electronic excitation with specific vibrational modes. The simulations show that when the difference in energy between the exciton and charge transfer orbitals matches the frequency of interfacial bond-stretching the energies of the orbitals start to oscillate in resonance. Moreover, charge transfer is only observed when these interfacial N-H bonds are free to move.

Parts of this chapter were published in:
T. J. Eisenmayer and F. Buda, "Real-time Simulations of Photoinduced Coherent Charge Transfer and Proton-Coupled Electron Transfer", *ChemPhysChem*, **2014**.
DOI: 10.1002/cphc.201402444

5.1 Introduction

In natural photosynthesis, photoinduced charge separation is the first fundamental step leading to the conversion of solar energy into chemical energy (see Chapters 3 and 4 of this thesis and [1,2]). There is converging experimental and theoretical evidence of oscillatory features associated with the reaction coordinates for energy and electron transfer in natural and artificial photosynthetic complexes (see Chapters 3 and 4 of this thesis and [3-9]). Understanding the nature and the role of this coherent dynamics is important both from a fundamental and technological point of view, as it may provide guiding principles for the design of efficient molecular devices for solar to fuel conversion. Photoinduced electron transfer processes are usually analysed in the context of transition rates. However, in reality many competing processes occur at the same time including dynamic and possibly coherent nuclear motion. Here we use instead Ehrenfest dynamics simulations to overcome this issue and investigate in real-time the coupling between the electronic motion and specific vibrational modes of the complex. We consider a donor-acceptor hydrogen bonded complex formed by melamine and isocyanuric acid that mimicks DNA base-pairing [10].

5.2 Model and Methods

For the time dependent Kohn-Sham (TDDFT) simulations of photoinduced electron transfer we consider a supramolecular complex consisting of melamine (1,3,5-triazine-2,4,6-triamine) and isocyanuric acid (1,3,5-triazine-2,4,6-trione) held together by a hydrogen bonding network (Figure 5.1) [11].

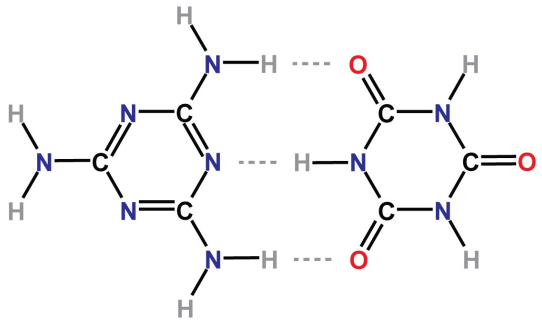

Figure 5.1: Melamine (donor; left) and isocyanuric acid (acceptor; right).

The biomimicry of the model lies in its resemblance with DNA base-pairing as it self-assembles into a tile-like structure with two-dimensional hydrogen bonds [11]. The geometry optimization of the complex is performed with the ADF program [12] at the BLYP/TZP level of theory. We do not impose the symmetry (C2v in this case); therefore even a small residual asymmetry at the end of the geometry optimization will manifest itself in the molecular orbitals. This can be seen in Figure 5.2 for the LUMO+2 that has no amplitude on the lower right amine, while it does on the top right amine.

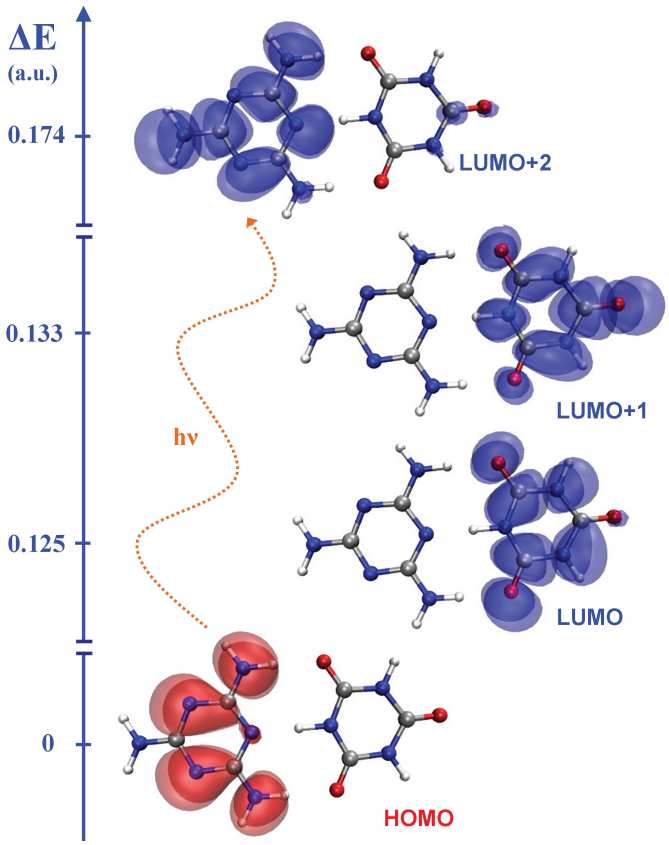

Figure 5.2: Localization of the frontier molecular orbitals at $t = t(0)$. The photoexcitation [HOMO]→[LUMO+2] and its energy are shown together with the gradients for photoinduced charge transfer [LUMO+2]→[LUMO+1/LUMO].

The optimized geometry is then used to perform a spin-polarized single-point LDA [13] density optimization on a real space grid with 52 Ry cutoff

using the OCTOPUS suite [14-17]. The core electrons are described by Troullier-Martins pseudopotentials in SIESTA format [18]. From the obtained set of occupied and unoccupied states we prepare the system in a single-particle excited state on the melamine, by depopulating the HOMO and populating the LUMO+2 (Figure 5.2). We also calculated the energies the relevant orbitals using different exchange-correlation functionals, including the Local-Density Approximation (LDA), a Generalized Gradient Approximation (BLYP) and several hybrid functionals with varying amount of Hartree-Fock exchange. We observe that the orbital energies involved in the photoinduced electron transfer process do not change significantly with respect to the Local-Density Approximation that is used to propagate the excitonic (HOMO $\rightarrow$ LUMO+2) state in time. In Table 5.1 we also report the oscillator strengths of the relevant excitations for the complex obtained using linear-response TDDFT calculations.

	BLYP	B3LYP	B1LYP	MPW1PW	CAM-B3LYP
Excitonic state (eV)	6.49	6.49	6.66	6.68	6.93
Oscillator strength	*0.295*	*0.191*	*0.274*	*0.269*	*0.597*
Charge Transfer state (eV)	3.57	4.79	5.11	5.14	6.45
Oscillator strength	*0.001*	*0.002*	*0.002*	*0.002*	*0.007*

Table 5.1: Linear-response TDDFT energies (eV) with different functionals.

We employ the BLYP and several hybrid functionals with varying amount of Hartree-Fock exchange. We also include the results obtained with the long-range corrected functional CAM-B3LYP that generally provides more accurate charge transfer excitation energies. Moreover, we have performed higher level ab initio calculations using the EOM-CCSD method with a cc-pVDZ basis set for the donor molecule. All these additional test calculations have been performed using the Gaussian 09 package [19]. We verify that across the range of functionals the excitonic state on the melamine has the highest oscillator strength. This justifies the [HOMO]$\rightarrow$[LUMO+2] excitation as the most appropriate starting condition for the excited state trajectories. For the excited state dynamics starting from the excitonic state, we solve the time dependent Kohn-Sham equations using the OCTOPUS quantum-chemical suite [14-17] with a time step of 2 attoseconds:

$$i\frac{\partial}{\partial t}\varphi_i(\boldsymbol{r},t) = \left[-{}^1\!/_2\nabla^2 + v_{eff}(\boldsymbol{r},t)\right]\varphi_i(\boldsymbol{r},t)$$
$$\sum_i^N |\varphi_i(\boldsymbol{r},t)|^2 = \rho(\boldsymbol{r},t). \tag{5.1}$$

This is achieved by constructing the time-dependent orbitals $\varphi(\boldsymbol{r},t)$ through an expansion of the adiabatic Kohn-Sham orbitals $\phi_i(\boldsymbol{r};\boldsymbol{R}(t))$ [20]:

$$\varphi(\boldsymbol{r},t)=\sum_i c_i(t)\phi_i(\boldsymbol{r};\boldsymbol{R}(t)). \tag{5.2}$$

To approximate the evolution operator we use the Approximated Enforced Time-Reversal Symmetry algorithm [17] and the exponential of the Hamiltonian is calculated by Taylor expansion. The nuclei are propagated classically within the Ehrenfest formalism on a mean-field potential energy surface [21]:

$$M_I\frac{d^2\boldsymbol{R}_I}{dt^2}=-\frac{\partial E_{KS}[\rho(\boldsymbol{r},t)]}{\partial \boldsymbol{R}_I}. \tag{5.3}$$

Nonadiabatic transitions between orbitals are invoked by evaluating the nonadiabatic coupling:

$$\boldsymbol{d}_{ij}=\langle\phi_i(\boldsymbol{r};\boldsymbol{R}(t))|\nabla_{\boldsymbol{R}}|\phi_j(\boldsymbol{r};\boldsymbol{R}(t))\rangle\cdot \mathrm{d}\boldsymbol{R}/\mathrm{d}t, \tag{5.4}$$

that modifies the coefficients $c_i(t)$ through [20]:

$$i\frac{\partial c_i(t)}{\partial t}=\sum_j c_j(t)(\epsilon_j\delta_{ij}-\boldsymbol{d}_{ij}), \tag{5.5}$$

To quantify the photoinduced electron transfer along the dynamics we monitor the photoinduced spin density (PSD):

$$PSD(r)=\rho^{\beta}(r)-\rho^{\alpha}(r)=\sum_i^{N/2}|\phi_i^{\beta}(r)|^2-\sum_i^{N/2}|\phi_i^{\alpha}(r)|^2 \tag{5.5}$$

where ρ represents the density, α and β the respective spin species, N the number of electrons and ϕ_i the Kohn-Sham molecular orbitals. Although the total spin of the system is equal to 0, the spatial spin distribution upon photoexcitation will show regions with an excess of α or β spin. By partitioning the simulation box in two halves, one containing the electron donor (melamine) and the other containing the electron acceptor (isocyanuric acid) we quantify the amount of PSD transferred through the hydrogen bond network. Furthermore, the negative/depleted regions of the PSD give the spatial localization of the photoinduced hole, whereas regions with an increase in PSD correspond to the photoinduced electron transfer.

5.3 Results and Discussion

To follow the photoinduced electron transfer through a hydrogen bond network we prepare the melamine cyanurate complex in a singlet excited state on the melamine. This represents a typical excitonic state where the electron and hole are both localized on the same moiety with no net charge transfer.

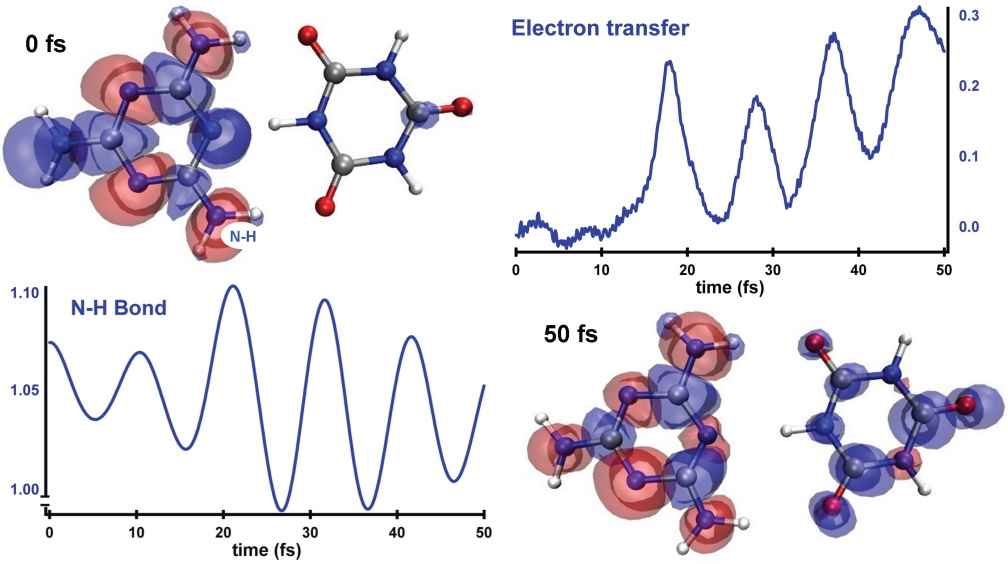

Figure 5.3: Coherent photoinduced electron transfer (upper right panel) in a DNA-base-pair-mimic held together by hydrogen bonds (See Movie **5.1**). The calculations were performed in real-time within the Ehrenfest formalism starting from the localized photoinduced spin density in the upper left panel. The photoinduced spin density after 50 fs (lower right panel) shows electron transfer (blue) to the isocyanuric acid and an accumulation of the hole (red) on the melamine. The fluctuations in the hydrogen bond network, illustrated by the N-H bond (Å) in the lower left panel, indicate a coherent coupling between proton displacements and electron transfer.

In terms of the photoinduced spin, we can compare the initial state of the quantum-classical dynamics (Figure 5.3, top left) with the involved orbitals (Figure 5.2) and verify that the depleted (red) density corresponds to the HOMO and the increase (blue) corresponds to the LUMO+2. Starting from the localized exciton state on the melamine the quantum-classical dynam-

ics simulation shows charge transfer through the hydrogen bond network with superimposed temporal oscillations with a period of approximately 10 fs (Figure 5.3, upper right panel). In wavenumbers this equals $\sim$ 3300 cm^{-1}, which lies in the amine N-H stretching mode range suggesting a coherent coupling of the (nonadiabatic) electron transfer with nuclear motion involving the hydrogen bond network. This is further illustrated by simply comparing the N-H bond dynamics (Figure 5.3, bottom left panel) with the oscillatory electron transfer along the trajectory, both exhibiting the same number of oscillations within the simulation time. The total charge transferred in 50 fs amounts to $\sim$ 0.3 electron equivalent. The dynamical snapshots in Appendix I show the photoinduced spin density along the dynamics where this oscillatory behaviour in the charge transfer is evident.

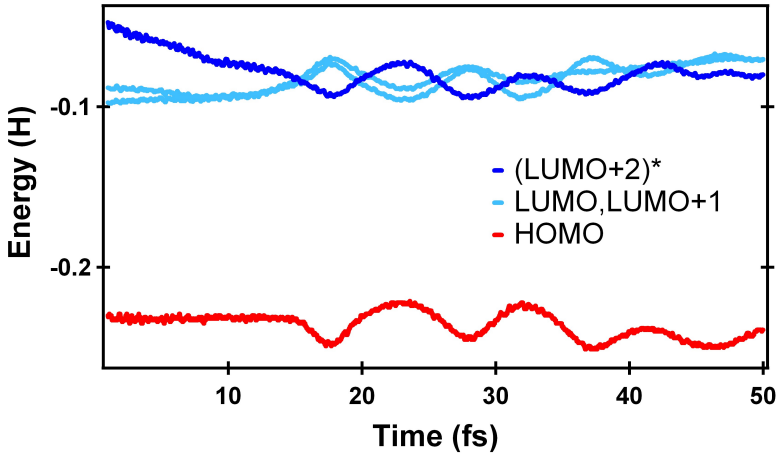

Figure 5.4: Eigenvalues of the molecular orbitals, the dark blue line represents the initially occupied excitonic LUMO+2, while the light blue lines represent the populated charge transfer orbitals LUMO and LUMO+1.

Interestingly, in Figure 5.4 it can be seen that the energies of the exciton (LUMO+2, dark blue line in Figure 5.4) and charge transfer states (LUMO+1,LUMO, light blue lines in Figure 5.4) oscillate in quasi-resonance once their difference matches the $\sim$ 3300 cm^{-1} energy of the N-H stretching vibration. This happens after approximately 10 fs, and is also the point where the charge transfer from the melamine donor to the isocyanuric acid acceptor is initiated (Figure 5.3, upper right panel). Therefore the coupling with the interfacial N-H stretching mode seems

crucial for there to be any charge transfer. We verify this by fixing the coordinates of the three interfacial N-H bonds and perform an identical dynamical evolution starting in the excitonic state. In this case the energies do not oscillate and do not cross as can be seen in Figure 5.5. Also, as can be seen from the dynamical snapshots in Apppendix II no charge is transferred from the melamine donor to the isocyanuric acid acceptor.

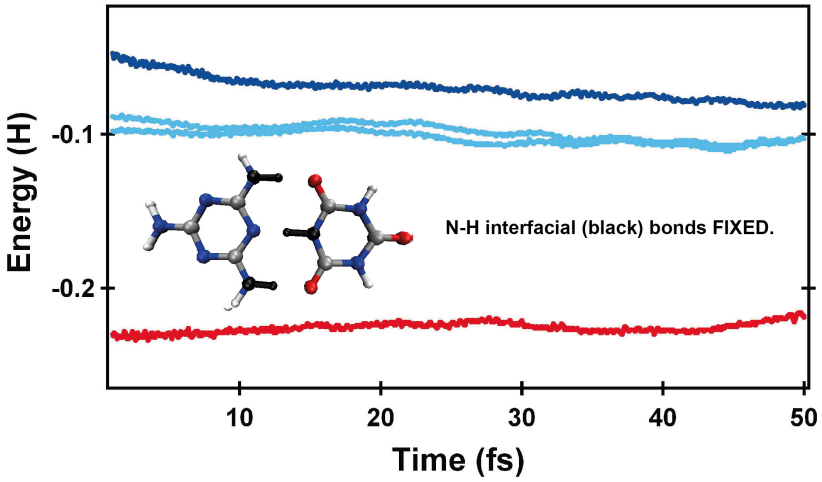

Figure 5.5: Eigenvalues of the molecular orbitals with the three interfacial N-H bonds (depicted in black) fixed, the dark blue line represents the initially occupied excitonic LUMO+2, while the light blue lines represent the charge transfer orbitals LUMO and LUMO+1. No charge transfer is observed.

In photosynthesis, coherent charge and energy transfer has been observed at ambient temperature in complex biological surroundings [3,4,8]. The near unity quantum yield of photon-to-charge conversion in photosynthetic complexes stems from such concerted nuclear motion of the chromophore and a responsive protein matrix [2,22]. The responsiveness lies in the fact that the matrix couples specific vibrations to the photoexcited chromophore that facilitate efficient photoinduced charge separation [3-5,9,23]. Promoting vibrations are also observed in enzyme catalysis [24] and proton displacements play an important role in facilitating electron transfer and preventing charge recombination in photosynthetic charge separation [23]. The coherent coupling between amine stretching vibrations and photoinduced electron transfer in melamine cyanurate (Figure 5.3) illustrates how proton

displacements control the charge transfer in a hydrogen bonded complex. It has recently been shown - with similar TDDFT/LDA simulations - that correlated, coherent motion of ions and electrons drives the first steps of photoinduced electron transfer in an artificial reaction center [7]. We show that even photoexcitation of a DNA base-pair mimic leads to such coherent motion. Based on these results we conclude that such characteristic vibrations involve the nuclear motion at the interface between donor and acceptor. It is tempting to suggest that this oscillatory behaviour is common to photoinduced charge transfer processes. A broader investigation on a range of supramolecular complexes is needed to verify the generality and role of this phenomenon. At the same time these coherences can be optimized to increase the efficiency of photon-to-charge conversion in molecular devices. Interestingly, our results show that when the vibration has an energy that matches the energy difference between exciton and charge transfer states, the charge transfer is initiated and the energies oscillate in quasi-resonance (Figure 5.4).

5.4 Conclusions

We have presented Ehrenfest dynamics simulations describing in real-time the electron transfer in melamine-cyanurate. The photoinduced ET dynamics in this DNA base-pair mimic shows an oscillatory behaviour that is suggested to be a signature of the coupling between electronic states and high frequency vibrational modes associated to hydrogen bonding interactions. When the nuclear coordinates associated to the N-H stretching modes are fixed no charge transfer occurs. We also observe that the transfer is initiated when the energy of the vibration matches the energy difference between exciton and charge transfer state. At this point, the energies are found to oscillate in quasi-resonance.

5.5 References

[1] D. Gust, T. A. Moore, A. L. Moore, Solar fuels via artificial photosynthesis, *Accounts of chemical research*, **2009**, 42, 1890.

[2] G. D. Scholes, G. R. Fleming, A. Olaya-Castro, R. van Grondelle, Lessons from nature about solar light harvesting, *Nature Chemistry*, **2011**, 3, 763-774.

[3] M. H. Vos, F. Rappaport, J. C. Lambry, J. Breton, J. L. Martin, Visualization of coherent nuclear motion in a membrane protein by femtosecond spectroscopy, *Nature*, **1993**, 363, 320-325.

[4] G. S. Engel, T. R. Calhoun, E. L. Read, T. K. Ahn, T. Mancal, Y. C. Cheng, R. E. Blankenship, G. R. Fleming, Evidence for wavelike energy transfer through quantum coherence in photosynthetic systems, *Nature*, **2007**, 446, 782.

[5] V. Novoderezhkin, A. Yakovlev, R. van Grondelle, V. Shuvalov, Coherent Nuclear and Electronic Dynamics in Primary Charge Separation in Photosynthetic Reaction Centers: A Redfield Theory Approach, *J. Phys. Chem. B*, **2004**, 108, 7445.

[6] A. W. Chin, J. Prior, R. Rosenbach, F. Caycedo-Soler, S. F. Huelga and M. B. Plenio, The Role of non-equilibrium vibrational structures in electronic coherence in pigment-protein complexes, *Nature Physics*, **2013**, 9, 113-118.

[7] C. A. Rozzi, S. M. Falke, N. Spallanzani, A. Rubio, E. Molinari, D. Brida, M. Maiuri, G. Cerullo, H. Schramm, J. Christoffers and C. Lienau, Quantum coherence controls the charge separation in a prototypical artificial light-harvesting system, *Nature communications*, **2013**, 4, 1602.

[8] Romero, E., Augulis, R., Novoderezhkin, V.I., Ferretti, M., Thieme, J., Zigmantas, D., and van Grondelle, R., Quantum coherence in photosynthesis for efficient solar-energy conversion, *Nature Physics* **2014**, *advanced publication*.

[9] Fuller, F.D., Pan, J., Gelzinis, A., Butkus, V., Senlik, S.S., Wilcox, D.E., Yocum, C.F., Valkunas, L., Abramavicius, D., and Ogilvie, J.P., Vibronic coherence in oxygenic photosynthesis, *Nature Chemistry* **2014**, 6, 706-711.

[10] Analysis of charge transfer effects in molecular complexes based on absolutely localized molecular orbitals, R. Z. Khaliullin, A. T. Bell, M. Head-Gordon, *J. Chem. Phys.*, **2008**, 128, 184112.

[11] L. M. Perdigao, N. R. Champness, P. H. Beton, Surface self-assembly of the cyanuric acid-melamine hydrogen bonded network, *Chem. Commun.*, **2006**, 5, 538-540.

[12] ADF2012, SCM, Theoretical Chemistry, Vrije Universiteit, Amsterdam, The Netherlands, http://www.scm.com/.

[13] J. P. Perdew and A. Zunger, *Phys. Rev. B*, **1981**, 23, 5048.

[14] X. Andrade, J. Alberdi-Rodriguez, D. A. Strubbe, M. J. T. Oliveira, F. Nogueira, A. Castro, J. Muguerza, A. Arruabarrena, S. G. Louie, A. Aspuru-Guzik, A. Rubio, and M. A. L. Marques, Time-dependent density-functional theory in massively parallel computer architectures: the octopus project, *J. Phys. Cond. Matt.*, **2012**, 24 233202.

[15] H. Castro, M. O. Appel, C.A. Rozzi, X. Andrade, F. Lorenzen, M.A.L. Marques, E.K.U. Gross, and A. Rubio, "Octopus: A tool for the application of time-dependent density functional theory", *Phys. Stat. Sol. B*, **2006**, 243, 2465-2488.

[16] M.A.L. Marques, Alberto Castro, George F. Bertsch, and Angel Rubio, "Octopus: a first-principles tool for excited electron-ion dynamics", *Comput. Phys. Commun.*, **2003**, 151, 60-78.

[17] Castro, M.A.L. Marques, and A. Rubio, Propagators for the time-dependent Kohn-Sham equations, *J. Chem. Phys.*, **2004**, 121, 3425-3433.

[18] N. Troullier and J. L. Martins, *Phys. Rev. B*, **1991**, 43, 1993-2006.

[19] M. J. Frisch, et al., Gaussian 09, Revision D.01; Gaussian, Inc.: Wallingford CT, **2009**.

[20] W. R. Duncan and O. V. Prezhdo, Nonadiabatic Molecular Dynamics Study of Electron Transfer from Alizarin to the Hydrated Ti^{4+} Ion, *J. Phys. Chem. B*, **2005**, 109, 17998-18002.

[21] X. Andrade, A. Castro, D. Zueco, J. L. Alonso, P. Echenique, F. Falceto and A. Rubio, Modified Ehrenfest Formalism for Efficient Large-Scale ab initio Molecular Dynamics, *J. Chem. Theor. Comp.*, **2009**, 5, 728-742.

[22] T.J. Eisenmayer, H.J.M. de Groot, E. van de Wetering, J. Neugebauer, F. Buda, Mechanism and Reaction Coordinate of Directional Charge Separation in Bacterial Reaction Centers, *J. Phys. Chem. Lett.*, **2012**, 3, 694.

[23] T. J. Eisenmayer, J. A. Lasave, A. Monti, H. J. M. de Groot, F. Buda, Proton Displacements Coupled to Primary Electron Transfer in the Rhodobacter sphaeroides Reaction Center, *J. Phys. Chem. B*, **2013**, 117, 38, 11162-11168.

[24] S. Hay, N. S Scrutton, Good vibrations in enzyme-catalysed reactions, *Nature Chemistry*, **2012**, 4, 161.

5.6 Appendix I

MOVIE 6.1: "Oscillatory Charge Transfer"

(Click below to see MOVIE)

Left top: Charge on the melamine. **Right top:** Charge on the cyanuric acid.
Bottom panel: Photoinduced spin density along the trajectory.

Appendix II

MOVIE 6.2: "Interfacial N-H bonds fixed: No Charge Transfer"

(Click below to see MOVIE)

Left top: Charge on the melamine. **Right top:** Charge on the cyanuric acid.
Bottom panel: Photoinduced spin density with interfacial N-H bonds fixed.